Investigating the spatial distribution of land surface temperature as related to air pollution level in Tehran metropolis

Saeedeh Nasehi | Ahmadreza Yavari✉ * | Esmail Salehi

School of Environment, College of Engineering, University of Tehran, Tehran, Iran

Article Info	ABSTRACT
Article type: Research Article **Article history:** Received: 11.09.2021 Revised: 02.02.2022 Accepted: 01.11.2022 **Keywords:** Surface temperature Interpolation Air pollutants Correlation Tehran	Urban Heat Island (UHI) is a common urban problem associated with a wide variety of factors, including air pollution. This study investigated the relationship between Land Surface Temperature (LST) and air pollution as two spatial phenomena affecting urban areas. LST was estimated from OLI sensor images taken on 01/07/2020 using the single-channel algorithm. Air pollution was assumed to be indicated by the concentrations of NOX, NO2, NO, PM2.5 and SO2, which were obtained by Inverse Distance Weighting (IDW) interpolation from the data recorded on the same date as satellite images. Correlations were measured in terms of R and R2 and errors were estimated in terms of RMSE, MAE and MBE. The highest R and R2 were obtained for SO2 (20.89 and 45.99, respectively). The results showed that despite the high correlation between SO2 and LST, PM2.5 has a much better error distribution. Therefore, further research should be conducted on the relationship between these indices.

INTRODUCTION

Rapid urbanization can sharply change a city's land cover and energy use intensity, causing a variety of environmental problems, most notably air pollution and the Urban Heat Island (UHI) effect (Singh et al., 2017; Wu et al., 2018).

In general, UHIs are caused by fast population growth and are associated with increasing air pollution (Owen & Peterson, 2005).

Fast urban population growth tends to cause a sharp spike in human activities, which manifests as considerable changes in land uses (McDonnell & MacGregor-Fors, 2016). It also increases the use of fossil fuels in vehicles, for cooking, and for heating or cooling buildings, which in turn increases the concentration of pollutants like sulfur dioxide (SO2), nitrogen dioxide (NO2), carbon monoxide (CO), and particulate matter (PM) in the city's atmosphere. These primary pollutants are major causes of poor air quality in urban areas. (Ghanbari Ghozikali et al., 2016; Khaniabadi et al., 2017). Air pollution has devastating effects on human health and is therefore considered a major global health issue. Many believe that air pollution is currently the most serious environmental hazard worldwide (Franchini et al., 2016; Mannucci & Franchini., 2017). Air pollution can trap heat and alter the city's radiation and energy balance. Some land covers can exacerbate these effects, leading to noticeable variations in the surface temperature of urban

*Corresponding Author Email: *ayavari@ut.ac.ir*

areas (Sachindra et al 2015; Connors et al., 2013). For example, atmospheric aerosols, which are essentially airborne liquid or solid particles produced by natural processes and human activities (Wong et al., 2009; Ziaul & Pal, 2018), can absorb heat, causing the atmosphere to become warmer in certain areas (Mahapatra et al., 2018).

In general, Land Surface Temperature (LST) is influenced by a multitude of factors, which include vegetation (Chen et al., 2011; Yang et al., 2017; Solangi et al., 2019), land use and its changes (Fu & Weng, 2016; Mukherjee & Singh., 2020; Kayet et al., 2016), Wind (Zhou et al., 2012; Xia et al., 2017; Zhou et al., 2013), altitude (Khandelwal et al., 2018; Phan et al., 2018; Malbéteau et al., 2017), urban geometry (Yang et al., 2015; Guo et al., 2016; Yang et al., 2021), and air pollution (Li et al., 2018; Zhang et al., 2016; Feng & Zou, 2019).

Temporal and spatial variations of UHI and air pollution are similar in some respects. For example, UHIs tend to be more intense in larger cities than in smaller ones, and air pollution tends to be worse in economically developed and densely populated urban areas than in other areas (Wu et al., 2018; Wang et al., 2021). Although air pollution and LST are both linked to urban land cover, the exact relationship between major air pollutants and LST (and therefore UHI) is not clearly understood. This relationship could be because of the higher energy consumption for air conditioning in the hotter areas of the city, which results in increased pollution (Weng & Yang, 2006).

Scientists have been collecting and analyzing records of surface air temperature for a long time. The world's first set of temperature estimates was compiled in 1938 by Callender, who after examining records collected from across the world, concluded that carbon dioxide from the burning of fossil fuels has been responsible for global warming over the preceding 50 years (Callender, 1938; Hawkins and Jones, 2013; Gillespie et al., 2021). In a 2021 study by Ngarambe et al. (2021), carbon monoxide (CO), nitrogen dioxide (NO2), sulfur dioxide (SO2), and particulate matter (PM) were found to be positively correlated with UHI intensity (HUII). However, a negative correlation was observed between UHII and ozone level (O3). These researchers also observed a significant seasonal effect in the strength of the correlation between UHI and air pollution. Their results also showed that these variations are affected by the sampling season and data collection time. In a study by Yoo et al. (2015) on the spatial and temporal variations of air pollutants (O3, NO2, SO2, CO, PM10, and VOCs) with four types of land use including residential (R), commercial (C), industrial (I) and green belt (G), the highest concentrations of air pollutants were found in daily, weekly and annual cycles of industrial areas for SO2 and PM10, commercial areas for NO2 and CO, and the green belt for O3. For all pollutants except O3, the concentration was higher in large cities on weekdays, but for O3, it was higher in suburban areas or small towns on weekends.

A study by Arvin (2018) on the relationship of UHI with air pollution in Isfahan found that UHI maps and pollution distribution maps were a match, showing higher temperatures in more polluted areas. This study found a significant correlation between pollution distribution and UHI, with higher correlation coefficients for days with higher pollution. In a study by Fang et al. (2021), they reported a positive correlation between the intensity of human activities and the level coupling effect, which they found to be a factor of certain spatial environment factors including residential, commercial, or industrial land use, the densities of road junctions and sub-arterial roads, type of buildings and their density, floor area ratio, and form ratio, and vegetation cover.

Najafzadeh et al. (2021) reported a positive correlation between air pollutants (NO2, O3, PM2.5, PM10) and UHI. In their study in Tabriz, Iran, Feizizadeh and Balashkeh (2013) found a significant relationship between land cover, LST, and PM10. In a study by Ranjbar and Bahak (2019) on the northeast of Tehran, they found a significant positive correlation between LST and carbon monoxide, nitrogen dioxide, and sulfur dioxide.

While all of the above studies have been on the subject of the correlation between UHI and

air pollution, their results suggest that more studies are still needed to measure the extent of this correlation. The findings of such studies can greatly facilitate the development of strategies to reduce air pollution and UHIs in urban areas, thereby improving the quality of urban air and micro-climate. This highlights the importance of further research into the relationship between LST and pollutants in urban areas with pollution and UHI problems.

MATERIALS AND METHODS

The city of Tehran is located between 51°06′-51°38′ east longitudes and 35°34′-35°51′ north latitudes. It is stretched from the southern slopes of the Alborz Mountains to the northern margins of the Dash-e-Kavir desert. As a result, the city's altitude decreases from about 1800 meters above sea level in the northernmost areas to 1200m in the central parts and 1050m in the south. With a population of about 11 million, Tehran is the most populous city in Iran and the 25th most populous city in the world. This city covers an area of about 731 square kilometers (Karimi et al., 2019). In general, Tehran has poor environmental conditions and most importantly a major air pollution problem, which in recent years has manifested as dangerously high concentrations of toxic pollutants and significant environmental and climatic changes (Bahari et al., 2015). Figure 1 shows a map of the study area.

In this study, pollutant concentration data including SO2, NOX, NO2, NO, PM2.5, which

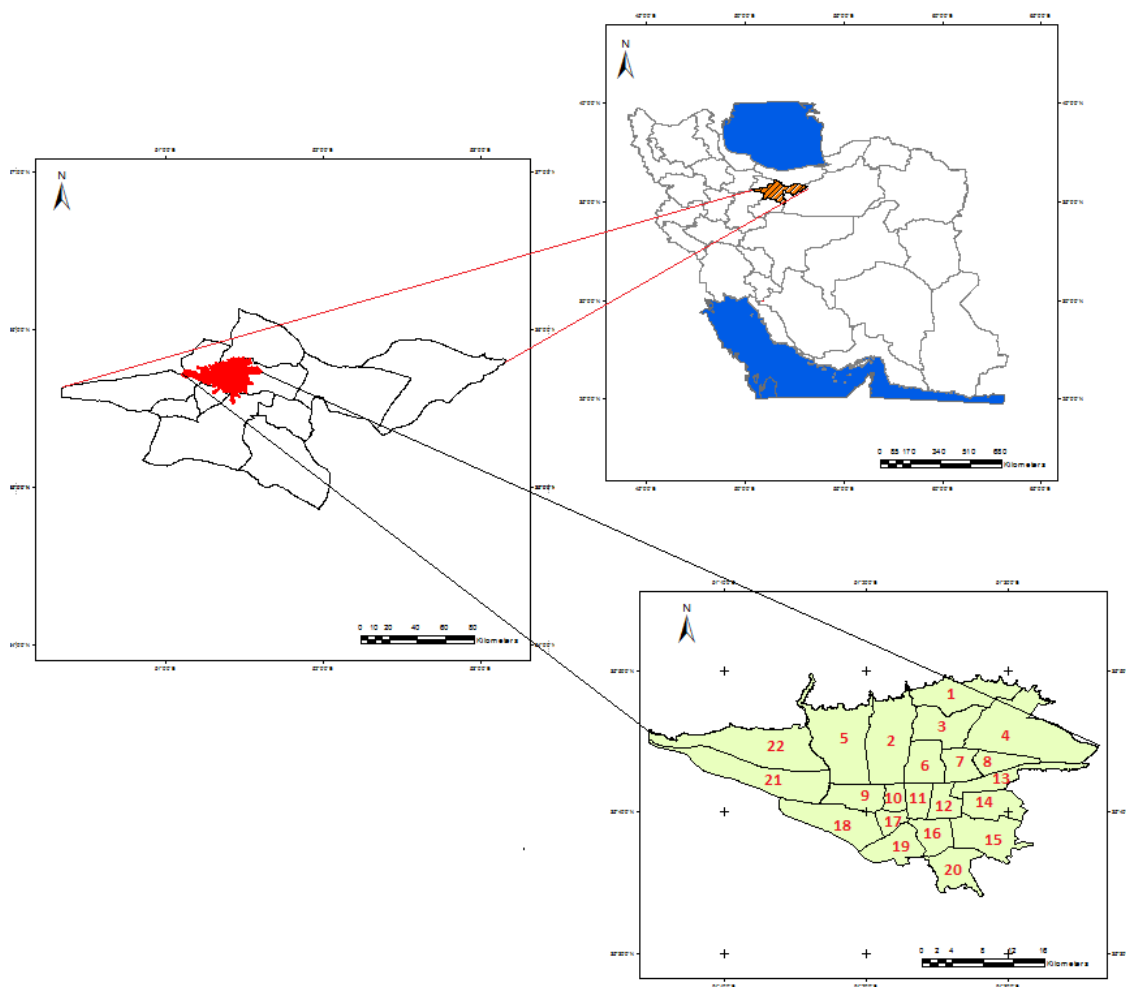**Fig. 1.** Map of the study area

Table 1. Specifications of the satellite image used in the study

Satellite	Sensor	Path/Row	Date
Landsat	TIRS	35/164	01/07/2020

were measured at the pollution measurement stations of the study area, were extracted from the website of the Tehran air quality control center, and were then used to prepare a distribution map for each pollutant by Inverse Distance Weighting (IDW) interpolation in the GIS software.

Inverse Distance Weighting (IDW) is one of the most widely used methods of interpolation. The main purpose of interpolation is to estimate the value of a parameter in areas where sampling has not been performed. This can be done by averaging the values of sampled points in the neighborhood of the unknown point. It is common to use the weighted average of known values for this purpose. Therefore, the weights assigned to the known points in the averaging operation could be quite important. In the IDW interpolation method, it is assumed that the effect of each known point is inversely proportional to the power P of its distance from the unknown point, which means the effect decreases as distance increases (Willmott & Matsuura, 1995).

In this study, Tehran's LST data were extracted from Landsat 8 satellite images taken on 01/07/2020. This satellite takes images in 11 spectral bands, of which bands 1 to 9, known as OLI (Operational Land Imager) bands, provide images in visible and near-infrared spectral range, and bands 10 and 11, known as TIRS (Thermal Infrared Sensor) bands provide images in the infrared range (Zante, 2016). After selecting the image, the part that was related to the study area was cropped and then subjected to pre-processing, including radiometric, geometric, and atmospheric corrections. LST estimation was then performed with the single-channel algorithm.

The specifications of the satellite image taken from the USGS website are provided in Table 1.

To convert raw images to interpretable LST data, it is necessary to perform some preprocessing and processing on these images by special digital image processing software. This includes obtaining spectral radiance, reflection coefficient, brightness temperature, land surface emissivity, and fractional vegetation cover.

LST estimation was performed using the generalized single-channel algorithm of Jimenez-Muñoz & Sobrino (2009).

This algorithm is one of the most accurate methods available for estimating LST. One of the important features of this method is the elimination of atmospheric effects. Also, since this algorithm uses both multispectral and thermal sensor data to estimate LST, it does not require detailed information about the atmospheric profile of satellite data (Wang et al., 1996).

In this algorithm, the following equation is used for all Landsat sensor data.

$$T_S = \gamma \left[\frac{1}{\varepsilon} \left(\psi_1 L_{sen} + \psi_2 \right) + \psi_3 \right] + \delta \qquad (1)$$

In this equation, Ts is the land surface temperature, ε is the land surface emissivity, and Lsen is the at-sensor radiance. The parameters γ and δ are obtained from Equation 2.

$$\gamma \approx \frac{T_{sen}^{\ 2}}{b_\gamma\, L_{sen}}; \qquad \delta \approx T_{sen} - \frac{T_{sen}^{\ 2}}{b_\gamma} \qquad (2)$$

where Tsen is the at-sensor brightness temperature, bγ is 1324 for Landsat 8, and ψ_1, ψ_2, and ψ_3 are the atmospheric functions, which, for Landsat 8, are obtained as follows:

$$\begin{bmatrix} \psi_1 \\ \psi_2 \\ \psi_3 \end{bmatrix} = \begin{bmatrix} 0.04019 & 0.02916 & 1.01523 \\ -0.38333 & -1.50294 & 0.20324 \\ 0.00918 & 1.36072 & -0.27514 \end{bmatrix} \begin{bmatrix} W^2 \\ W \\ 1 \end{bmatrix} \tag{3}$$

c_{ij} coefficients must be obtained by simulation, and W is the atmospheric water vapor.

Multivariate linear regression was used to investigate the relationship between LST and each pollutant. This method is commonly used to analyze how changes in one, two, or more independent variables affect the changes of an independent variable. In this analysis, the goal is to determine the simultaneous effect of several independent variables on a target variable. The general form of this model is defined as follows.

$$y = \beta_0 + \sum_{k=1}^{p} \beta_k \, x_{k+\varepsilon} \tag{4}$$

In Equation (4), y is the dependent variable, $\beta 0$ is the intercept, βk denotes the coefficients of the regression model, xk denotes independent variables, ε is the curve fitting error, and k is the number of independent variables.

In this study, regression coefficients were obtained using the least-squares method, as it is the most widely used method for fitting a straight regression line to observations. This method finds the best fit for a set of observed points by minimizing the sum of squares of vertical offsets of these points from the regression line (Ganesh et al., 2010).

The correlation coefficient (r) varies from -1 to 1. r=1 indicates a direct or positive relationship between the two variables, meaning that when one variable increases (decreases), the other also increases (decreases). r=-1 indicates an inverse or negative relationship between the two variables, meaning that when one variable increases, the other variable decreases, and vice versa. r=0 indicates that there is no linear relationship between the two variables.

The coefficient of determination (R2) is the statistical measure of how close the data are to the fitted regression line. This coefficient indicates what percentage of variability of the dependent variable is explained by the independent variable, or in other words, how much of the variations in the dependent variable is affected by the relevant independent variable and how much of it is related to other factors.

Another parameter for measuring the correlation between independent and dependent variables is the Pearson coefficient. This coefficient is calculated by the following equation (Equation 5).

$$R = \frac{\sum (X - \overline{x})(y - \overline{y})}{\sqrt{(x - \overline{x})^2 - \sum (y - \overline{y})^2}} \tag{5}$$

where X and Y are the values of the two variables and $\overline{x}$ and $\overline{Y}$ are their averages.

There are several criteria for evaluating and validating statistical methods like linear regression. In this study, RMSE, MAE, and MBE were used for this purpose. These criteria are defined in Equations 6 to 8.

Root Mean Square Error (RMSE) is commonly used as a measure of the difference between observations and model predictions . RMSE is sensitive to both random errors and systematic errors. This measure is calculated by Equation 6:

$$RMSE = \sqrt{\frac{1}{n} \sum_{i=1}^{n} (pridict - Ground)^2} \tag{6}$$

where n is equal to the total number of data, Predict is the value predicted by the model, and Ground is the observed value in the ground data. A lower RMSE indicates the better accuracy of the model.

Mean Absolute Error (MAE) is a widely used measure of average error. MAE can be obtained from Equation 7 (Sadidi et al., 2017).

$$MAE = \frac{1}{n} \sum_{i=1}^{n} | \, pridict - Ground \, | \qquad (7)$$

where X and Y are the values of the two variables and $\overline{x}$ and $\overline{Y}$ are their averages.

For Mean Bias Error (MBE), positive values indicate that model predictions are overestimates (higher than the actual values) and negative values indicate that they are underestimates (lower than the actual values) (Nosrati et al., 2007). This measure is given by Equation 8.

$$MBE = 1/n \sum_{i=1}^{n} \left(pridict - Ground \right) \qquad (8)$$

After determining the relationship between pollutant distribution and LST by regression, fuzzy OR, AND, SUM, PRODUCT, and GAMMA operators were used to combine pollutant distribution maps into multi-pollutant overlay (MPO) maps based on a degree of membership defined for each pollutant layer. This process was carried out in the ARC GIS software.

The output of the AND operator is the lowest value of the standardized fit measure, which means it selects the most appropriate fit. The output of the OR operator is the highest value of the standardized fit measure, which means it ignores low membership values.

The Fuzzy SUM and PRODUCT operators are the fuzzy versions of algebraic summation and multiplication operators. These operators have maximum increasing and maximum decreasing tendencies, and typically cannot provide a reliable result alone. These operators are used in the fuzzy GAMMA operator.

The GAMMA operator combines the PRODUCT and SUM operators based on a weight called γ, which ranged from 0 to 1. When γ=1, the GAMMA operator is the same as algebraic summation, and when γ=0, this operator functions as algebraic multiplication (Atkinsona et al., 2005).

RESULTS AND DESCUTION

The present study investigated the temporal and spatial relationship between UHI and air pollutants in Tehran using Landsat 8 satellite images by analyzing the linear regression correlation between LST and pollutant concentrations. The LST map of Tehran produced using the single-channel method based on the images taken on 01/07/2020 is presented in Figure 2.

As the LST map shows, the northern parts of the city tend to have lower LSTs than other parts and the UHI effect tends to increase from north to south. The city's western expanses also have a significantly higher number of UHIs than the middle and eastern parts. The western parts of the city have no notable urban cool islands except Chitgar Lake but contain several major UHIs. Table 2 shows the area of each LST class as a percentage of the city's total area.

As Table 2 shows, the LST class of <35°C constitutes slightly over 1% of the city's area, which is a very small percentage. The LST class of 35-40°C makes up a much larger portion of the city (over 35%). However, the largest LST class in terms of area is 40-45°C, which constitutes about 40% of the city's area. Temperatures of 40-45°C are uncomfortably hot and are unbearable for many people including the elderly, children, and people with certain diseases. The two hottest LST classes (i.e. >45°C), which are problematic and unbearable for many people, span over
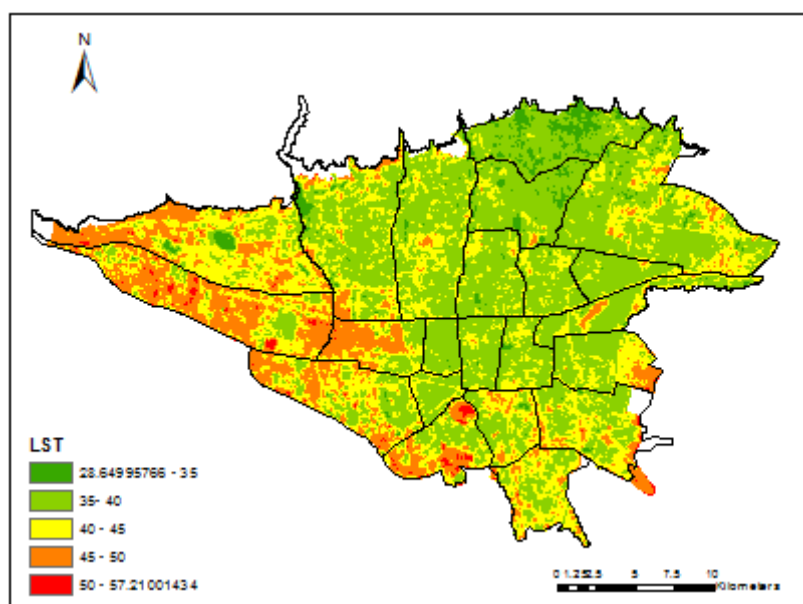
Fig. 2. LST map of Tehran

Table 2. Percentage area of LST classes in Tehran

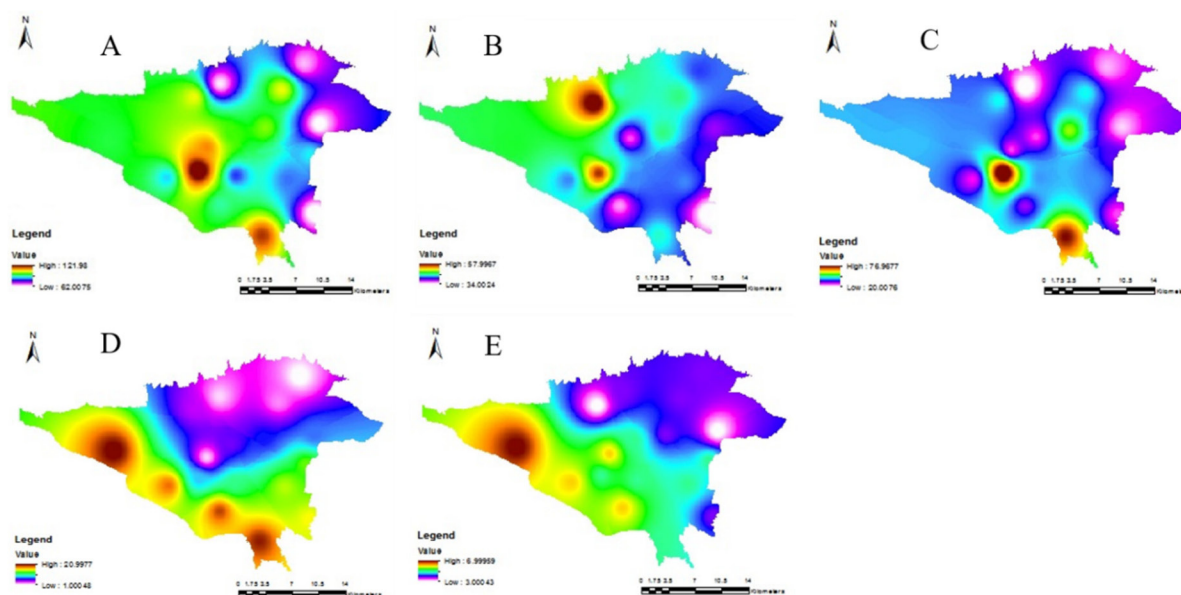| LST class (°C)	29-35	35-40	40-45	45-50	>50
Percentage of city's total area	1.01%	35.32%	40.42%	20.47%	2.78%

Fig. 3. Interpolated pollution map of Tehran A) NOX, B) NO2, C) NO, D) PM2.5, E) SO2

almost a quarter of the city.

In this study, air pollution was investigated in terms of NOX, NO2, NO, PM2.5 and SO2. Figure 3 shows the NOX, NO2, NO, PM2.5, and SO2 maps of Tehran produced by IDW interpolation.

In Figure 3, the pollution maps of the study area are plotted separately for each pollutant.

In these maps, the level of pollution is indicated by a continuous spectrum of colors from dark brown to pale purple and white. Brown indicates high concentrations of pollutants and purple and white indicates low concentrations of pollutants in the environment. As Figure 3-A shows, NOX concentrations are lowest in the northern, northeastern, and southeastern parts of the city and highest in its southern, central and southwestern parts. In Figure 3-B, it can be seen that NO2 concentrations are highest in the northern and southwestern parts and lowest in the southern, northeastern and southeastern parts. NO concentrations are lowest in the northern and northeastern sections and parts of the center, southwest and southeast, and highest in the southern expanses and part of the southwest (Figure 3-C). As Figure 3-D shows, PM2.5 concentrations are highest in the northern and central parts of the city and lowest in the southern, southwestern, and northwestern parts. In Figure 3-E, one can see that SO2 concentrations are highest in very small areas in the central and southwestern parts of the city and in much larger areas in the northwestern parts. The lowest SO2 concentrations are in the northern and southeastern parts of the city.

According to the maps illustrated in Figure 3, the northern and northeastern parts of the city have the lowest levels of pollution in terms of almost all indices, but especially NO, PM2.5 and SO2. As these results indicate, the northern parts of the city have cleaner air than other parts. Overall, the analysis of the maps of Figure 3 suggests that the pollution situation is worst (highest pollutant concentrations) in the western parts of Tehran, followed by the southern parts and central parts.

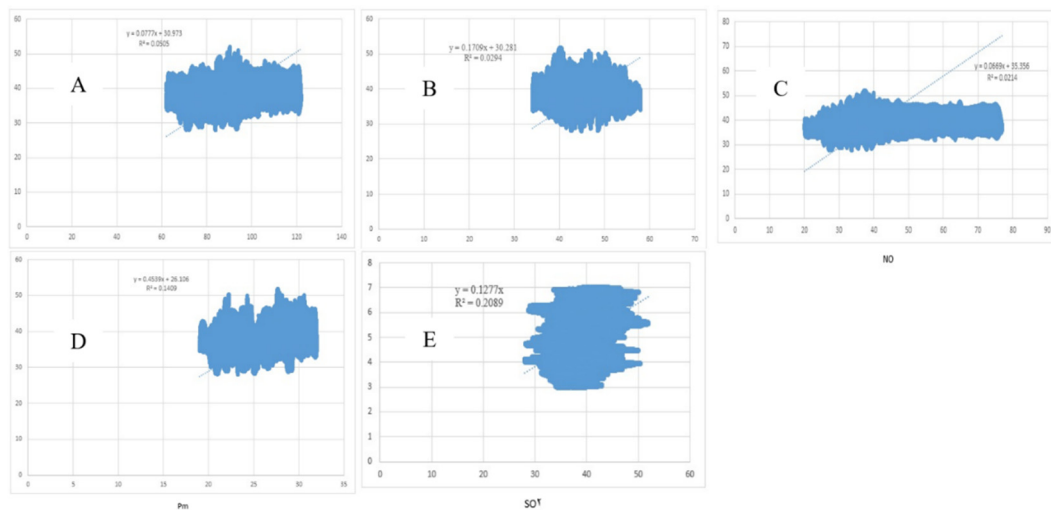Figure 4 and Table 3 show the relationship between LST and air pollution indices in Tehran

Fig. 4. Relationship between LST and pollution indices A) NOX, B) NO2, C) NO, D) PM2.5, E) SO2

Table 3. Correlation results for the relationship between pollutants and LST and the corresponding error values

Measure	Pollutant				
	NOX	NO₂	NO	PM₂.₅	SO₂
R	22.47	17.49	14.62	37.54	45.99
R²	5.05	2.94	2.14	14.09	20.89
RMSE	13.12	3.23	3.23	3.03	7.35
MAE	12.06	2.6	2.67	2.44	6.68
MBE	-0.04	0.0006	-0.0004	0.0003	0.02

based on the analysis of the data.

As shown in Figure 4, the highest coefficients of determination (R2) for the relationship between pollution indices and LST were obtained for SO2 (R2=20.89) and PM2.5 (R2=14.09), and the lowest were obtained for NO (R2=2.14) and NO2 (R2=2.94). In general, it can be concluded that among the pollutants, SO2 has the highest correlation with LST. Table 3 shows the relationship between pollution indices and LST based on correlation measures along with the corresponding error values.

As Table 3 shows, SO2 has better correlation values than other pollutants (its Pearson coefficient is about 46 and its coefficient of determination is about 20.9), but PM2.5 has better error rates than other pollutants

The multi-pollutant overlay maps produced by overlaying the pollutant distribution maps by different fuzzy operators are illustrated in Figure 5.

From the maps produced by the five operators (AND, OR, SUM, PRODUCT, and GAMMA0.5), the one obtained from the AND operator was selected for use in the next stage. This map was selected because of the greater strictness and capability of the AND operator in differentiating the most and least polluted areas. Using this operator, the study area was classified into five zones: very high pollution, high pollution, moderate pollution, low pollution, and very low pollution. The multi-pollutant overlay map produced with this operator is shown in Figure 6.

For easier comparison of LST and pollution situation of the 22 districts of Tehran, the distribution of pollution classes and the average LST in each of these 22 districts are plotted in Figure 7 and Figure 8, respectively.

By comparing the multi-pollutant overlay map and the LST map, we can see that District 21, which has the highest average LST (44.87°C), also has the highest pollution, as 98.02% of this district falls in the "very high pollution" class. The second and third most polluted districts are District 18 and District 19, with respectively 91.24% and with 87.11% of their area falling in the "very high pollution" class. These two districts have an average LST of 42.91°C and 43.37°C, respectively, which are quite high. According to a study by Hereher et al. (2021) on Shubra
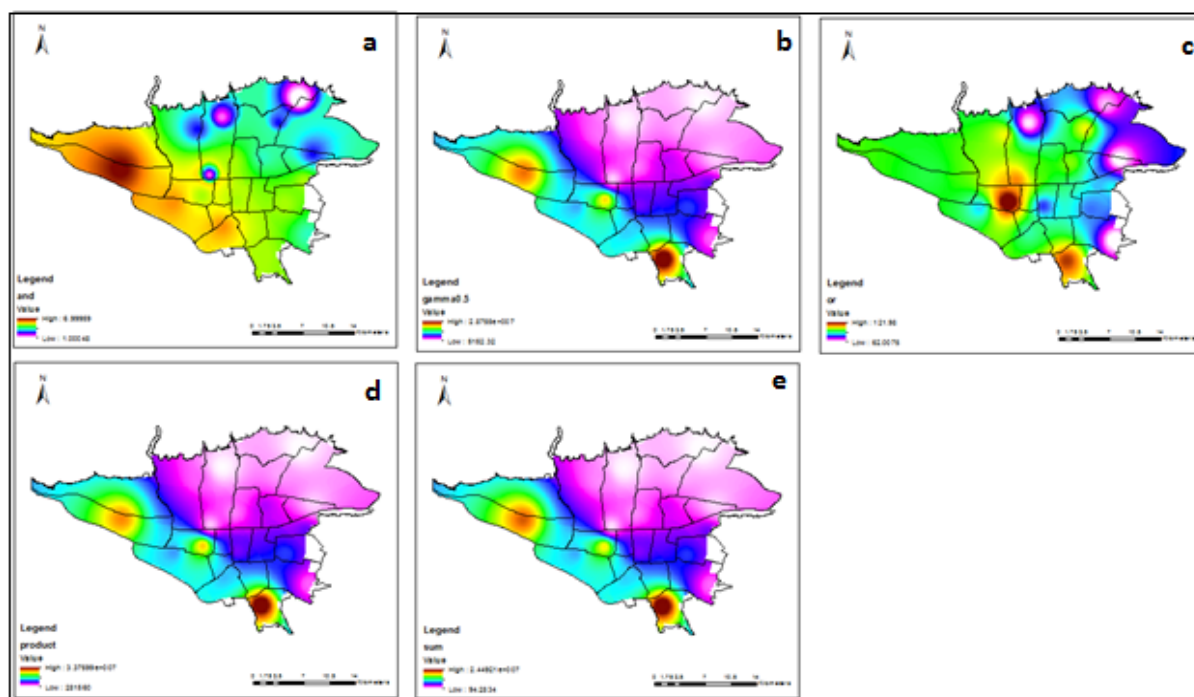

Fig. 5. Multi-pollutant overlay maps produced by fuzzy operators: a) AND b) Gamma0.5 c) Or d) Product e) Sum
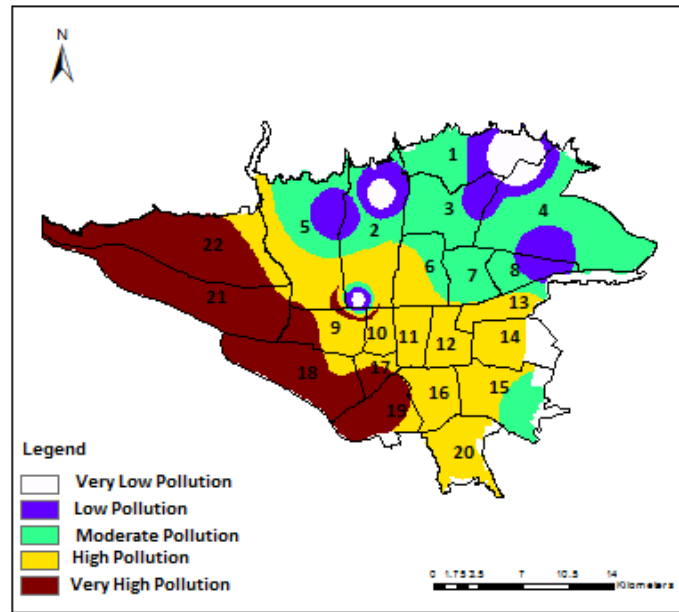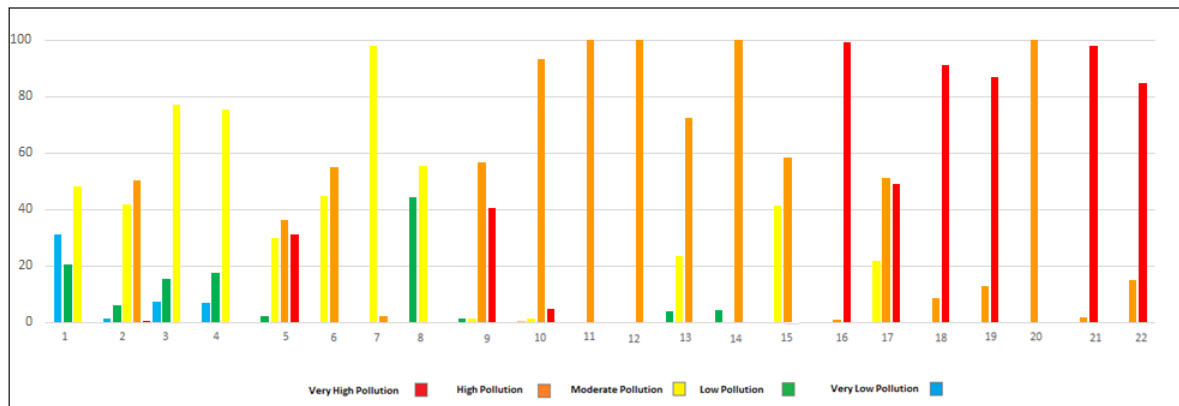
Fig. 6. Multi pollutant overlay map of Tehran

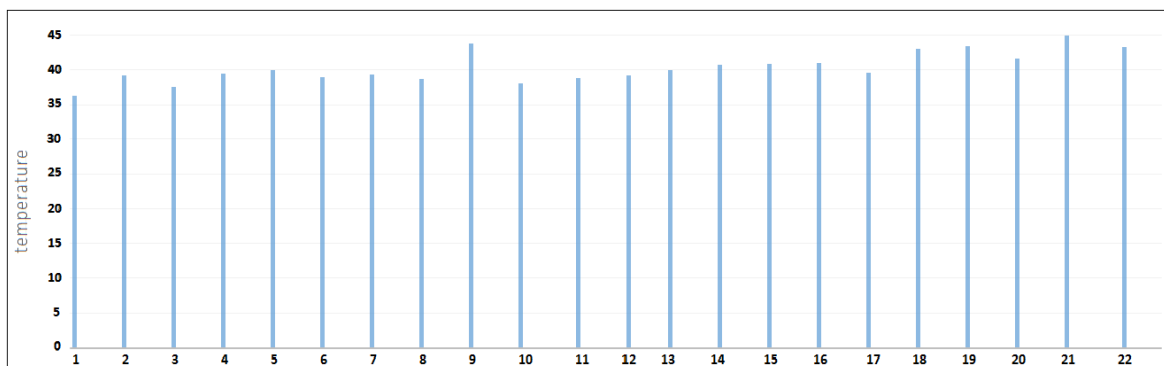**Fig. 7.** Distribution of pollution classes in the 22 districts of Tehran

Fig. 8. Average LST in the 22 districts of Tehran

al-Khaymah (a northern suburb of Cairo), high concentrations of SO2 in urban areas could be due to the extensive use of diesel trucks in the construction of new asphalt roads as well as industrial facilities, chemical and petrochemical plants, and transportation. In the present study, the highest SO2 concentrations were observed in the western and southwestern parts of the city, and particularly District 21, which is a mostly industrial area.

The study of Hereher et al. (2021) also showed high NO2 concentrations near Cairo Airport. Consistent with this finding, in the present study, the highest NO2 concentration was observed near Mehrabad Airport in District 9, which also has the second-highest LST after District 21.

In a study by Zhang et al. (2020) in China, they attributed the temporal-spatial variations of PM2.5 concentration to the presence of industrial centers, including steel factories, and stated that these industries are major fossil fuel consumers and inevitably emit huge amounts of greenhouse gases. For Tehran, the main reasons for this pollution could be the presence of fossil fuel burning industries as well as increasing urbanization and transportation. Industrial sources are likely to be the main cause of high PM2.5 concentration in Districts 18, 19, and 21, where there is a high concentration of such industries. The high concentration of PM2.5 is one of the main causes of the extensive UHI effect in the western, southern, and southwestern parts of Tehran. A study by Matkan et al. (2009) in Tehran metropolis also concluded that industrial activities are the most important source of PM pollution in this area. In the present study, a correlation was observed between LST and the concentration of particulate matter smaller than 2.5 microns, which, according to Matkan et al. (2009) is mainly produced by industrial sites in these districts. The PM2.5 distribution map of Tehran (Figure 3) also shows the high concentration of this pollutant in these districts.

In a study by Etabi et al. (2007), they stated that the main cause of pollution in District 22 is particulate matter, which is consistent with our findings, (Figure 3). In the present study, 85% of this district fell in the "very high pollution" class and it had an average LST of over 43.31°C, which was the fourth-highest among all districts.

A study by Wang et al. (2021) showed that UHI and air pollution are influenced by factors like geographical location, altitude, and economic development level. These researchers observed lower air pollution in areas located at higher altitudes and also in coastal and near-water areas compared to residential areas. The present study also observed higher LST in the southern parts of Tehran (which have lower altitudes) than in the northern parts (Figure 8). A major reason for this difference is the altitude difference between the city's northern parts, which are positioned on foothills, and its southern parts, which are mostly situated on plains (in Tehran, altitude generally decreases from north to south). Topographical differences could also be a major cause of LST and pollution variations.

The results showed a noticeable drop in LST near Chitgar Lake in the west of Tehran (Figure 2), which is consistent with the findings of Wang et al. (2021) in China.

The present study also found a significant correlation between pollutants and LST, which is in good agreement with the results of Ranjbar and Bahak (2019) and Ngarambe et al. (2021).

CONCLUTION

The subject of this study was the relationship between air pollution and LST in Tehran. To investigate this relationship, the LST map of Tehran was prepared from Landsat 8 images taken on 01/07/2020 using the single-channel method. LST analysis results showed that urban cool islands (<35°C) make up a very small portion (about 1%) of the city's area, and over 23% of the entire city has LSTs above 45°C, which could be dangerous for many of the residents.

It is indeed important to establish whether there is a significant relationship between air pollution and LST, because if such a relationship really exists, it will mean that the adverse impacts of high air temperatures can be alleviated by controlling air pollution. In this study, the

air pollution situation was favorable in the city's northern parts and to some extent northeastern part, but was unfavorable in most other parts, especially in the city's western expanses. The next most polluted sections of the city were its central and southern parts. The main causes of high pollution in the western parts of Tehran include the presence of heavy industries and a major airport in these areas.

The results of this study showed a direct relationship between air pollutants and LST, meaning that they increase and decrease with each other. This relationship can even be visually observed in the produced pollutant and LST maps, most notably in that the city's northern parts, which have the lowest LST, also have the lowest concentrations of pollutants and on the contrary of the city's western parts have the highest LST as well as the highest concentrations of pollutants. Among the five pollutants examined as pollution indices, SO2 and PM2.5 had the highest correlation with LST. It should be noted that although SO2 had the highest correlation values, it also had the second-highest error values after NOX. This shows that while SO2 can predict air temperature with generally high accuracy, the error of predictions in a few areas will be quite high. In other words, the standard deviation of SO2-based temperature predictions will be high. While PM2.5 has a lower correlation with LST than SO2, it has the lowest error rates among all indices. This means that while PM2.5 may not be as accurate in predicting temperature, it does offer certainty that predictions will be equally accurate over the entire city area.

Comparing the LST map of Tehran with the pollutant concentration maps showed that in all maps, the situation generally gets worse (LST increases and pollutant concentration increases) as we move from north to south. The city's western and southern parts, which have high concentrations of most pollutants, also have the highest temperatures, and the city's northern parts, where pollutant concentrations are lower, are also colder than other parts.

For future studies, the authors recommend examining the relationship between UHI and air pollution in chronological and seasonal order, as there is a general consensus that pollutant concentrations tend to be higher in spring and winter than in other seasons.

GRANT SUPPORT DETAILS

CONFLICT OF INTEREST

The authors declare that there is not any conflict of interests regarding the publication of this manuscript. In addition, the ethical issues, including plagiarism, informed consent, misconduct, data fabrication and/ or falsification, double publication and/or submission, and redundancy has been completely observed by the authors.

LIFE SCIENCE REPORTING

No life science threat was practiced in this research.

REFERENCES

Atabi, F., Karbasi, A., Haji, M. H. S. and Abbaspour, M. (2007). Modeling the emission of particulate matter using ADMS-Urban. J. Environ. Sci. Technol, 9(1), 1-15.

Atkinson, D. M., Deadman, P., Dudycha, D. and Traynor, S. (2005). Multi-criteria evaluation and least cost path analysis for an arctic all-weather road. Applied Geography, 25(4), 287-307.

Callender, G. (1938). The artificial production of carbon dioxide and its influence on temperature. Q J R

Meteorol Soc, 64, 223– 240.

Chen, Y., Yang, K., He, J., Qin, J., Shi, J., Du, J. and He, Q. (2011). Improving land surface temperature modeling for dry land of China. J. Geophys Res. Atmos, 116 (D20).

Fang, Y. and Gu, K. (2021). Exploring coupling effect between urban heat island effect and PM2. 5 concentrations from the perspective of spatial environment. Environ. Eng. Res.1-32

Feng, H. and Zou, B. (2019). Satellite-based estimation of the aerosol forcing contribution to the global land surface temperature in the recent decade. Remote Sens. Environ, 232, 111299.

Feizizadeh, B. and Blaschke, T. (2013). Land suitability analysis for Tabriz County, Iran: a multi-criteria evaluation approach using GIS. J. Environ. Plan. Manag, 56(1), 1-23.

Franchini, M., Mengoli, C., Cruciani, M., Bonfanti, C. and Mannucci, P. M. (2016). Association between particulate air pollution and venous thromboembolism: A systematic literature review. Eur. J. Intern. Med, 27, 10-13.

Fu, P. and Weng, Q. (2016). A time series analysis of urbanization induced land use and land cover change and its impact on land surface temperature with Landsat imagery. Remote Sens. Environ, 175, 205-214.

Ganesh, K. S., Unnikrishnan, B., Nagaraj, K. and Jayaram, S. (2010). Determinants of pre-eclampsia: a case control study in a district hospital in South India. Indian J. Community Med: official publication of Indian Association of Preventive & Social Medicine, 35(4), 502.

Ghozikali, M. G., Heibati, B., Naddafi, K., Kloog, I., Conti, G. O., Polosa, R. and Ferrante, M. (2016). Evaluation of chronic obstructive pulmonary disease (COPD) attributed to atmospheric O3, NO2, and SO2 using Air Q Model (2011–2012 year). Environ. Res., 144, 99-105

Gillespie, I. M., Haimberger, L., Compo, G. P. and Thorne, P. W. (2021). Assessing potential of sparse-input re-analyses for centennial-scale land surface air temperature homogenization. Int J Climatol, 41, E3000-E3020.

Guo, G., Zhou, X., Wu, Z., Xiao, R. and Chen, Y. (2016). Characterizing the impact of urban morphology heterogeneity on land surface temperature in Guangzhou, Environ Model Softw, 84, 427-439.

Hawkins, E. and Jones, P.D. (2013) On increasing global temperatures: 75 years after Callendar. Q. J. R. Meteorol. Soc, 139, 1961–1963.

Hereher, M., Eissa, R., Alqasemi, A., El Kenawy, A.M. (2021). Assessment of air pollution at Greater Cairo in relation to the spatial variability of surface urban heat island. Environ. Sci. Pollut. Res, 1-14.

Jiménez-Muñoz, J. C. and Sobrino, J. A. (2009). A single-channel algorithm for land-surface temperature retrieval from ASTER data. IEEE Geosci. Remote. Sens. Lett, 7(1), 176-179.

Karimi, A., Pahlavani, P. and Bigdeli, B. (2019). Determining affective factors on land surface temperature of Tehran using Landsat images and integrating geographically weighted regression with genetic algorithm. J. Geo Spat Inf Tech, 7(3), 79-102

Kayet, N., Pathak, K., Chakrabarty, A. and Sahoo, S. (2016). Spatial impact of land use/land cover change on surface temperature distribution in Saranda Forest, Jharkhand. Model. Earth Syst. Environ, 2(3), 1-10.

Khandelwal, S., Goyal, R., Kaul, N. and Mathew, A. (2018). Assessment of land surface temperature variation due to change in elevation of area surrounding Jaipur, India. Egypt. J. Remote Sens. Space Sci, 21(1), 87-94.

Khaniabadi, Y. O., Daryanoosh, S. M., Amrane, A., Polosa, R., Hopke, P. K., Goudarzi, G. and Armin, H. (2017). Impact of Middle Eastern Dust storms on human health. Atmos. Pollut. Res, 8(4), 606-613.

Li, H., Meier, F., Lee, X., Chakraborty, T., Liu, J., Schaap, M. and Sodoudi, S. (2018). Interaction between urban heat island and urban pollution island during summer in Berlin. Sci. Total Environ, 636, 818-828.

Mahapatra, P. S., Sinha, P. R., Boopathy, R., Das, T., Mohanty, S., Sahu, S. C. and Gurjar, B. R. (2018). Seasonal progression of atmospheric particulate matter over an urban coastal region in peninsular India: role of local meteorology and long-range transport. Atmos. Res, 199, 145-158.

Matkan, A. A., Shakiba, A. R., Purali, S. H. and Baharloo, I. (2009). Determination of spatial variation of CO and PM10 air pollutants, using GIS techniques (case study: Tehran, Iran) Remote Sens. GIS, 1(1), 57-72.

Malbéteau, Y., Merlin, O., Gascoin, S., Gastellu, J. P., Mattar, C., Olivera-Guerra, L., ... & Jarlan, L. (2017). Normalizing land surface temperature data for elevation and illumination effects in mountainous areas: A case study using ASTER data over a steep-sided valley in Morocco. Remote Sens Environ, 189, 25-39.

Mannucci, P. M. and Franchini, M. (2017). Health effects of ambient air pollution in developing

countriesInt. J. Environ. Res. Public Health, 14(9), 1048.

McDonnell M.J., MacGregor-Fors I. The ecological future of cities. Sci, 2016, 352, 936-938

Mukherjee, F. and Singh, D. (2020). Assessing land use–land cover change and its impact on land surface temperature using LANDSAT data: A comparison of two urban areas in India. Earth Syst and Environ, 4(2), 385-407.

Najafzadeh, F., Mohammadzadeh, A., Ghorbanian, A., Jamali, S., (2021). Spatial and Temporal

Analysis of Surface Urban Heat Island and Thermal Comfort Using Landsat Satellite Images between 1989 and 2019: A Case Study in Tehran. Remote Sens, 1-25.

Ngarambe, J., Jeong Joen, S., Han, G., Yun, G. (2021). Exploring the relationship between particulate matter, CO, SO2, NO2, O3 and urban heat island in Seoul, Korea. J. Hazard. Mater. 1-13.

Nosrati, K., Zehtabian, G. R., Moradi, E.,& Shahbazi, A (2008), Evaluation of stochastic Simulation method for generating meteorological data, Geogr. Res.Q.J. 1-9.

Peterson, T.c. and Owen, T.W. (2005). Urban heat island assessment: Metadata are important. J. Clim, 18(14) 2637-2646

Phan, T. N., Kappas, M. and Tran, T. P. (2018). Land surface temperature variation due to changes in elevation in northwest Vietnam. Clim, 6(2), 28.

Qin, Z.; Karnieli, A.; Berliner, P. A. (2001). Mono-window algorithm for retrieving land surface temperature from landsat tm data and its application to the Israel-Egypt border region. Int. J. Remote Sens., 22, 3719–3746.

Ranjbar, M. and Bahak, B. (2019). Time and Space Changes of Air Pollutants Using GIS (Case Study: North Semnan Tehran. J Geog, 17(60), 72-85.

Sadidi, Javad, Rezaian, Hani, Borshan, Mohammad Reza (2017), Comparison of error distribution in recursive artificial neural networks Elman and Jordan in estimating the concentration of atmospheric particulate matter (PM10) using satellite imagery (MODIS Case Study: Ahvaz City, 17 (47). 155-169.

Solangi, G. S., Siyal, A. A. and Siyal, P. (2019). Spatio-temporal dynamics of land surface temperature and its impact on the vegetation. Civ. Eng. J, 5(8), 1753-1763.

Wang, Y., Guo, Zh. Han, J. (2021). The relationship between urban heat island and air pollutants and them with influencing factors in the Yangtze River Delta, China. Ecol. Indic, 1-10.

Willmott, C. J. and Matsuura, K. (1995). Smart interpolation of annually averaged air temperature in the United States. Appl Meteorol Climatol, 34(12), 2577-2586.

Wong, M., Nichol, J., Lee, K. H. and Li, Z. (2009). High resolution aerosol optical thickness retrieval over the Pearl River Delta region with improved aerosol modelling. Sci. China, D Earth sci, 52(10), 1641-1649.

Xia, G., Cervarich, M. C., Roy, S. B., Zhou, L., Minder, J. R., Jimenez, P. A. and Freedman, J. M. (2017). Simulating impacts of real-world wind farms on land surface temperature using the WRF Model: Validation with observations. Mon Weather Rev, 145(12), 4813-4836.

Yang, J., Menenti, M., Wu, Z., Wong, M. S., Abbas, S., Xu, Y. and Shi, Q. (2021). Assessing the impact of urban geometry on surface urban heat island using complete and nadir temperatures. Int J Climatol, 41, E3219-E3238.

Yang, J., Sun, J., Ge, Q. and Li, X. (2017). Assessing the impacts of urbanization-associated green space on urban land surface temperature: A case study of Dalian, China. Urban For Urban Green, 22, 1-10.

Yang, J., Wong, M. S., Menenti, M. and Nichol, J. (2015). Study of the geometry effect on land surface temperature retrieval in urban environment. ISPRS J. Photogramm. Remote Sens, 109, 77-87.

Yoo, J. M., Jeong, M. J., Kim, D., Stockwell, W. R., Yang, J. H., Shin, H. W., ... & Lee, S. D. (2015). Spatiotemporal variations of air pollutants (O 3, NO 2, SO 2, CO, PM 10, and VOCs) with land-use types. Atmos. chem. phys, 15(18), 10857-10885.

Zhang, J., Reid, J. S., Christensen, M. and Benedetti, A. (2016). An evaluation of the impact of aerosol particles on weather forecasts from a biomass burning aerosol event over the Midwestern United States: observational-based analysis of surface temperature. Atmos. Chem. Phys, 16(10), 6475-6494.

Zhou, L., Tian, Y., Roy, S. B., Dai, Y. and Chen, H. (2013). Diurnal and seasonal variations of wind farm impacts on land surface temperature over western Texas. Clim Dyn, 41(2), 307-326.

Zhou, L., Tian, Y., Roy, S. B., Thorncroft, C., Bosart, L. F. and Hu, Y. (2012). Impacts of wind farms on land surface temperature. Nat Clim Change, 2(7), 539-543.

Ziaul, S. and Pal, S. (2018). Analyzing control of respiratory particulate matters on Land Surface Temperature in local climatic zones of English Bazar Municipality and Surroundings. Urban Clim, 24, 34-50.